Stance-Phase Detection for ZUPT-Aided Foot-Mounted Pedestrian Navigation System

Zhelong Wang, *Member, IEEE*, Hongyu Zhao, Sen Qiu, and Qin Gao

***Abstract*—Zero velocity updates (ZUPT) is an effective way for the foot-mounted inertial pedestrian navigation systems. For the ZUPT technique to work properly, it is necessary to correctly detect the stance phase of each gait cycle. An adaptive stance-phase detection method is proposed based solely on an inertial sensor, which deals with the measurement fluctuations in swing and stance phases differently, and applies a clustering algorithm to partition the potential gait phases into true and false clusters, thereby yielding a time threshold to eliminate the false gait phases. The roles of the detection parameters and the relationship between them are analyzed to offer some suggestions for parameter tuning. Detection performance is evaluated with multisubject experimental data collected at varying walking speeds. The evaluation results show that the proposed detection method performs well in the presence of measurement fluctuations, which can make the detection of stance phases more robust and the choice of detection parameters more flexible.**

***Index Terms*—Inertial measurement unit (IMU), inertial navigation system (INS), pedestrian navigation system (PNS), stance-phase detection, zero velocity updates (ZUPT).**

I. Introduction

In environments where GPS or beacon signals are degraded or unavailable, tracking and locating an object is a challenging issue [1]–[3]. Self-contained pedestrian navigation systems (PNS) constructed of small inertial measurement units (IMU) have been developed for this purpose. Such systems can work in arbitrary unfamiliar and unprepared indoor and outdoor environments, and have been attracting increasing interests in medical, commercial, and safety-specific applications.

However, because of the integrative nature of the inertial navigation systems (INS), any small errors will accumulate and grow without bound [4]–[6]. The position estimate of free-inertial navigation features a cubic-in-time error growth that may diverge over a short period of time, especially when using the low-cost IMUs. Fortunately, a foot-mounted INS aided by the zero velocity updates (ZUPT) technique has the ability to bound the navigation errors. The elegance of ZUPT lies in the fact that the foot swings to stance phase periodically during most types of human locomotion, such as walking, running, and ascending or descending stairs. In ideal conditions, the foot is stationary during the stance phase. However, as the IMUs inevitably suffer from drift, the velocity estimate never shows exactly zero. In practical applications, if any kind of velocity is not zero, it is treated as the velocity error generated during the gait cycle. This information can be effectively exploited by the ZUPT technique.

Extensive research has been performed to put the ZUPT into practical use. The INS-derived velocity was directly reset to zero during the stance phase in [7] and [8]. The velocity error was introduced as pseudomeasurement into the Kalman-type filters in [9] and [10]. The filtering ZUPT can achieve additional benefit of reducing other navigation errors that are correlated with the velocity error, such as position error, attitude error, and sensor bias errors. Instead of resetting the navigation errors only during the stance phase, Feliz *et al.* implemented the ZUPT by applying a velocity bias error to recalculate the velocity during both swing and stance phases [11]. A similar ZUPT implemented by Yun *et al.* applied an acceleration bias error to correct the acceleration during the swing phase [12].

The stance phase is the time period during which the ZUPT can be applied to the system. Extra sensors in addition to the IMU have been used to aid the stance-phase detection, such as radio frequency sensors, cameras, and pressure sensors [8], [13], [14]. Although the extra sensors might help to improve the detection accuracy, they increase the system cost and complexity, and make the system more sensitive and less ubiquitous. Besides, it is confirmed by other authors' study and our ongoing study that some external measurements will not necessarily improve the system performance [15]. The work described in this paper is based solely on the IMU.

Generally, the stance phase can be detected by using either measurements of the gyroscope or accelerometer alone or both in combination. The angular velocity was used alone in the form of magnitude [10], root mean square [16], and moving average [17]; the acceleration was used alone in the form of magnitude [18], moving average [19], and moving variance [20]; both measurements were used in [9] and [21]. Good detection results can be achieved using both measurements; however, the detection method using one of the measurements also performs well. Different detection methods have been compared in [22], and the results suggest that angular velocity is more reliable than acceleration for typical walking, which is supported by [11], [12] and our study. In this paper, only the angular velocity is used to detect the stance phase.

To use the ZUPT technique properly, the stance phase should be correctly detected. However, the existing detection methods either do not examine the false or interrupted stance phases at all, or directly filter out all the short stance phases indiscriminately, which makes the detection results sensitive

Manuscript received September 14, 2013; revised December 19, 2014 and March 12, 2015; accepted March 28, 2015. Date of publication May 6, 2015; date of current version October 21, 2015. Recommended by Technical Editor O. Kaynak. This work was supported by the National Natural Science Foundation of China under Grant 61174027 and Grant 61473058, National High Technology Research and Development Program (863 program) Project (2012AA041505-02), and Fundamental Research Funds for the Central Universities (DUT15ZD114). *(Corresponding author: Hongyu Zhao.)*

The authors are with the School of Control Science and Engineering, Dalian University of Technology, Dalian 116024, China (e-mail: wangzl@dlut.edu.cn; zhy.lucy@hotmail.com; qantasy@gmail.com; onlygaoqin@gmail.com).

Color versions of one or more of the figures in this paper are available online at http://ieeexplore.ieee.org.

Digital Object Identifier 10.1109/TMECH.2015.2430357

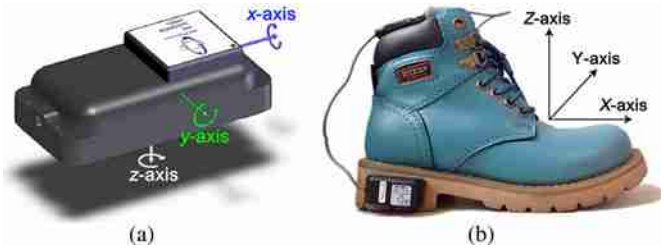

Fig. 1. Hardware setup of the PNS. (a) Memsense nIMU. (b) Attachment of the nIMU.

TABLE I
KEY SPECIFICATIONS OF MEMSENSE NIMU

Mass (grams)		20
Size (mm)		45 × 23 × 13
Gyroscope	Range (deg/s)	±600
	Offset (deg/s)	±1.5
	Noise (deg/s)	0.56 (0.95)
	Bandwidth (Hz)	50
Accelerometer	Range (g)	±5
	Offset (mg)	±30
	Noise (mg)	1.1 (1.3)
	Bandwidth (Hz)	50

to measurement fluctuations and detection parameters. To our knowledge, no measurement fluctuation that interrupts the stance phase has been examined, no relationship between the detection parameters has been discussed, and no treatment of adaptively tuning any detection parameter has been reported.

The main study of this paper is to develop an adaptive stance-phase detection method, which can eliminate the false gait phases induced by the measurement fluctuations in both swing and stance phases. The influence of measurement fluctuations on the stance-phase detection is investigated over a wide parameter space, together with the importance of eliminating this influence for enhancing the system performance.

II. ZUPT-AIDED IPNS IMPLEMENTATION

In this section, we give a brief description of the system hardware, the coordinate frames, and the algorithm structure.

A. System Hardware

The hardware setup of our system is shown in Fig. 1. The inertial sensor used in this system is the Memsense Nano IMU (nIMU for short), a low-cost, small-size, and low-weight MEMS unit [23]. For testing on different users, the sensor is externally attached to the heel of the user's boot. The nIMU is compensated for temperature sensitivities to bias and scale factor, and its key manufacturer specifications are listed in Table I. The data are acquired and stored through the Memsense IMU Data Console, which allows basic data display and collection using the RS422 protocol. The sampling rate is 150 Hz, which is three times the sensor bandwidth.

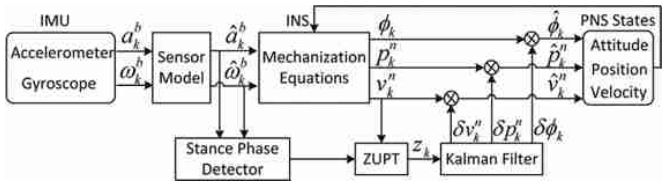

Fig. 2. Software setup of the PNS.

B. System Coordinate

For the pedestrian navigation purpose, two coordinate frames are introduced, which are as follows.

1) The body coordinate frame (b-frame for short) is parallel to the sensor's axes shown in Fig. 1(a).
2) The navigation coordinate frame (n-frame for short) is a local east-north-up reference frame shown in Fig. 1(b).

As seen in Fig. 1, the b-frame has an initial roll angle of approximately 90° about the X-axis of the n-frame. All the IMU data are measured in the b-frame, while all the INS states are calculated in the n-frame.

C. System Software

The software presented in this paper has six modules: sensor model, INS module, stance-phase detector, Kalman filter, ZUPT module, and INS error corrector as shown in Fig. 2. The functionalities of these modules are described below.

1) Sensor Model: The sensor model corrects the raw IMU measurements by compensating for the bias and scale errors

$$\begin{aligned} \hat{\omega}_k^b &= K_G \left(\omega_k^b - \varepsilon^b\right) \\ \hat{a}_k^b &= K_A \left(a_k^b - \nabla^b\right) \end{aligned} \tag{1}$$

where k is the sampling index, ω_k^b is the raw angular velocity, a_k^b is the raw acceleration, ε^b is the gyroscope bias, ∇^b is the accelerometer bias, K_G is the gyroscope scale factor, K_A is the accelerometer scale factor, $\hat{\omega}_k^b$ is the compensated angular velocity, and $\hat{a}_k^b$ is the compensated acceleration.

2) INS Module: The INS algorithm integrates the compensated IMU measurements to estimate the raw INS states by solving the discrete-time navigation equations

$$\begin{aligned} C_{b_k}^n &= C_{b_{k-1}}^n \left[(2I_{3\times 3} + \Omega_k \Delta t)/(2I_{3\times 3} - \Omega_k \Delta t)\right] \\ v_k^n &= v_{k-1}^n + \left(C_{b_k}^n \hat{a}_k^b + g^n\right) \Delta t \\ p_k^n &= p_{k-1}^n + \left(v_{k-1}^n + v_k^n\right) \Delta t/2 \end{aligned} \tag{2}$$

where Δt is the sampling period, $C_{b_k}^n$ is the attitude matrix, Ω_k is the skew-symmetric matrix of $\hat{\omega}_k^b$ used to update the attitude matrix, g^n is the gravitational acceleration, v_k^n is the velocity, and p_k^n is the position.

3) Stance-Phase Detector: The stance-phase detector uses the compensated IMU measurements to generate a logic signal for activating the ZUPT when the foot is in its stance phase as detailed in the next section.

4) Kalman Filter: The Kalman filter acts as an indirect filter to estimate the errors of the raw INS states. The process model

of the Kalman filter is designed based on the simplified INS error model

$$\begin{aligned}\delta\dot{\phi} &= -C_b^n \delta\omega^b \\ \delta\dot{v}^n &= \left(C_b^n \hat{a}^b\right) \times \delta\phi + C_b^n \delta a^b \\ \delta\dot{p}^n &= \delta v^n \end{aligned} \tag{3}$$

where $\delta\phi$ is the attitude error, δv^n is the velocity error, δp^n is the position error, $\delta\omega^b$ is the gyroscope measurement error, and δa^b is the accelerometer measurement error.

As given in (2) and (3), due to the poor error characteristics of low-cost IMUs and the limited speeds and distances of pedestrian movements, the full navigation equations and the full navigation error models have been simplified by neglecting some physical effects, such as the Earth's rotation and curvature, the Coriolis force, and the centrifugal force.

Then, the continuous-time error model can be discretized as

$$\delta x_k = F_k \delta x_{k-1} + w_{k-1} \tag{4}$$

where $\delta x_k = [\delta\phi_k, \delta v_k^n, \delta p_k^n]$ is the error state vector, F_k is the state transition matrix, and w_{k-1} is the process noise.

Although some variants of the Kalman filter (extended, unscented, or adaptive Kalman filters) are commonly used to implement the ZUPT for foot-mounted IPNS [9], [24], a standard Kalman filter is used in this study, since the error dynamics given by (3) can be well represented by a linear model. To reduce the modeling error, no sensor measurement errors are modeled in the Kalman filter, because completely stationary state of the foot rarely occurs during normal walking and the quality of the stance-based pseudomeasurements is generally too poor to estimate such errors, even though the sensor biases are usually modeled [8], [9], [24].

5) ZUPT Module: When activated, the ZUPT method treats the raw velocity as a pseudomeasurement of the velocity error and feeds it into the Kalman filter via the measurement model

$$z_k = H\delta x_k + \eta_k \tag{5}$$

where $H = \begin{bmatrix} 0_{3\times3} & I_{3\times3} & 0_{3\times3} \end{bmatrix}$ is the measurement matrix, z_k is the aiding measurement derived from v_k^n, and η_k is the measurement noise.

The Kalman filter prediction is performed at each INS estimation step, whereas the Kalman filter update is performed only when the aiding measurement is available.

6) INS Error Corrector: The error corrector utilizes the error estimates to refine the raw INS states by

$$\begin{aligned}\hat{C}_{b_k}^n &= \left[(2I_{3\times3} + \Theta_k)/(2I_{3\times3} - \Theta_k)\right] C_{b_k}^n \\ \hat{v}_k^n &= v_k^n - \delta v_k^n \\ \hat{p}_k^n &= p_k^n - \delta p_k^n \end{aligned} \tag{6}$$

where $\hat{C}_{b_k}^n$ is the corrected attitude matrix, Θ_k is the skew-symmetric matrix of $\delta\phi_k$ used to refine the attitude matrix, $\hat{v}_k^n$ is the corrected velocity, and $\hat{p}_k^n$ is the corrected position. As given in (2) and (6), a first order Padé approximation is used to update and correct the attitude matrix.

The Kalman filter is applied in a closed-loop manner, which means that the error estimates are used to correct the INS states after each filtering step. The error estimates are not propagated over time but reset to zero every time the correction is made.

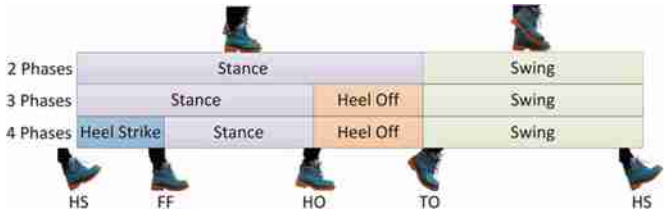

Fig. 3. Key events and phases of the gait cycle.

III. Stance-Phase Detection Method

In this section, the common ways of dividing a gait cycle are first surveyed, then the existing stance-phase detection methods are discussed, and finally, an adaptive stance-phase detection method is proposed.

A. Gait Cycle Division

There are four typical events in one normalized gait cycle: heel-strike (HS), foot-flat (FF), heel-off (HO), and toe-off (TO). Usually, the HS event is specified as the start of a gait cycle, and a complete gait cycle is defined as the time interval between successive HS events of the same foot. The common ways of dividing a gait cycle are shown in Fig. 3. The first way divides a gait cycle into four phases, and the stance phase lasts from FF to HO corresponding to about 30% of the gait cycle [25]. The second way divides a gait cycle into three phases, and the stance phase is delimited by HS and HO constituting about 40% of the gait cycle [26]. The third way divides a gait cycle into stance and swing phases, and the stance phase lasts from HS to TO comprising about 60% of the gait cycle [11]. In this study, a gait cycle is also divided into two phases. The stance phase is the same as that in the first division with the foot entirely on the ground, while the swing phase lasts from HO to FF when any part of the foot is in the air, so better to call it a nonstance phase.

As each individual has a unique gait pattern, the percentage of the gait cycle spent in each phase slightly varies between the literature sources. For an adult walking at normal cadence of 100–120 steps/min, the stance phases last around 0.3 s, which is deemed sufficient for the ZUPT technique to correct the navigation errors.

Since the IMU is attached to the user's foot, the acceleration and angular velocity exhibit periodic patterns. A segment of the raw IMU measurements is shown in Fig. 4, together with the corresponding gait phases and their percentages. It can be observed that the angular velocity has more prominent features than the acceleration in terms of the gait event indication. The acceleration features sudden spikes when the HS and TO events occur, which may induce momentary measurement fluctuations and result in false detections of the gait phases. By contrast, the angular velocity is relatively smoother.

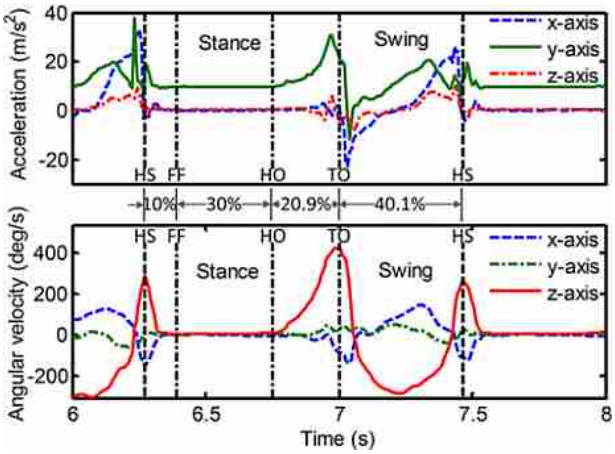

Fig. 4. IMU measurements with corresponding gait events and gait phases.

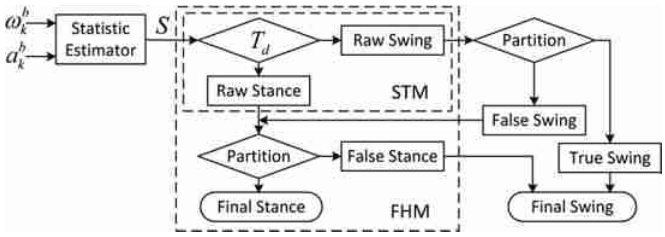

Fig. 5. Block diagram of the adaptive stance-phase detection method.

B. Detection Method Analysis

Based on the above discussion, the stance-phase detection seems to be a pattern recognition process, where the pattern being looked at satisfies the following two conditions:

1) Acceleration condition: $\|\hat{a}_k^b\| = g$;
2) Angular velocity condition: $\|\hat{\omega}_k^b\| = 0$

where $\|\cdot\|$ is the two-norm of the vector, and g is the magnitude of the gravitational acceleration.

The detection method allows the state transition between the stance and swing phases. The most common stance-phase detection methods can be divided into two categories. The first is the single detection threshold method, which first calculates the short-term statistic of the IMU measurements for a given window size, and then, compares it with a predefined detection threshold to distinguish the stance and swing phases [10], [24]. A stance phase can be declared if

$$S\left(\left\{a_k^b, \omega_k^b\right\}|W\right) < T_d \tag{7}$$

where $S(\cdot)$ is the detection statistic, W is the window size, and T_d is the detection threshold.

The second is the fixed time heuristic method, which adds a time duration threshold to the first method, and filters out the raw stance phases that have a duration shorter than the time threshold [12], [20]. A stance phase can be declared if

$$L\left(S\left(\left\{a_k^b, \omega_k^b\right\}|W\right) < T_d\right) > \Delta t \tag{8}$$

where $L(\cdot)$ is the time duration, and Δt is the time threshold.

In practice, there are not only measurement dips during the swing phase with detection statistic lower than the detection threshold, but also measurement rises during the stance phase with detection statistic higher than the detection threshold, both of which can result in false detections of the gait phases. The first method is simple but does not take the measurement fluctuations into consideration. The second method also has its own disadvantages: first, the time threshold is hand tuned, which may work well for the measurements that it is derived from, but does not apply to each person's individual data; second, this method directly filters out all the short stance phases, without treating them differently according to their causes. In the cases when the measurement rise breaks a stance phase down into short subphases, the second method not only fails to play its due role, but even performs worse than the first method. Therefore, a single detection threshold or combined with a fixed time threshold is not sufficient to correctly detect the stance phases. In this paper, an adaptive detection method is proposed. For convenience, the detection methods are abbreviated as follows.

1) STM: Single detection threshold method.
2) FHM: Fixed time heuristic method.
3) ADM: Adaptive detection method.

The proposed method has two interactive branches: a swing branch and a stance branch as shown in Fig. 5. The swing branch first partitions the raw swing phases into true and false groups. Then, the confirmed false swings are restored to their stance state to ensure the integrity of the stance phases, and this is achieved by merging the false swing phases and the raw stance phases into a new group of stance phases. The stance branch finally partitions the potential stance phases into true and false groups. By this means, the interrupted stance phases are restored and the false stance phases are filtered out. Using a clustering technique, an adaptive time threshold can be found to distinguish the true and false gait phases. The dashed rectangles in Fig. 5 indicate that the STM and FHM methods realize only part of the functionality of the ADM method. The ADM method can detect the stance phases more robustly, and further facilitate the choice of other detection parameters as discussed in the following sections.

IV. Stance-Phase Detection Parameter

In this paper, the angular velocity energy is used to derive the detection statistic, which is defined as

$$S_{\omega_k} = S\left(\omega_k^b \left| \left\{W, \sigma_\omega^2\right\}\right.\right) = \frac{1}{\sigma_\omega^2 W} \sum_{j=k}^{k-W+1} \left\|\omega_j^b\right\|^2 \tag{9}$$

where σ_ω^2 is the gyroscope noise variance, which has no effect on the detection performance but acts as a scaling factor.

In total, three interrelated parameters are involved in the stance-phase detection: the window size W, the detection threshold T_d, and the time threshold Δt as detailed in this section. Note that the defined detection statistic S_ω is a dimensionless measure, and so is the detection threshold T_d.

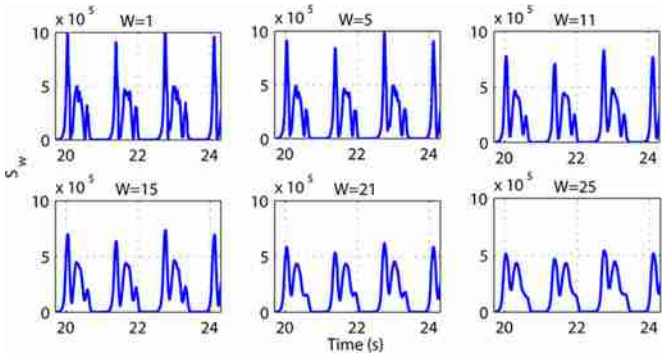

Fig. 6. Detection statistic S_ω versus window size W. The window size W is the number of samples over which the detection statistic S_ω is calculated.

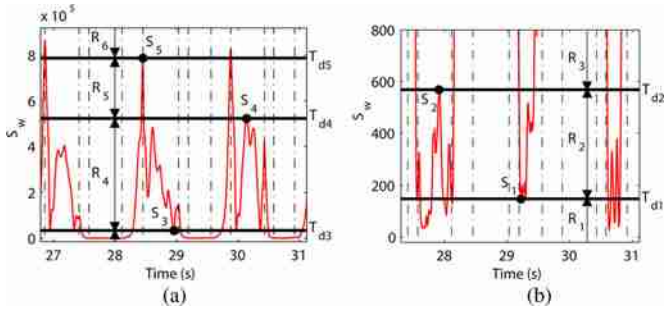

Fig. 7. Detection statistic S_ω versus detection threshold T_d. (a) Large key detection thresholds. (b) Small key detection thresholds. (b) Close-up view of (a). The dash-dotted lines indicate the typical gait events.

A. Window Size Parameter

As given in (9), the detection statistic S_ω can be regarded as a function of the window size W. For comparison purposes, S_ω is calculated for varying W, and six of them are shown in Fig. 6. As seen in Fig. 6, the statistic estimator can function as a filter to smooth the measurement fluctuations and highlight the gait cycles. The larger the window size, the smoother the detection statistic. However, due to the algorithmic delay of $W/2$, S_ω has a slow response to the measurement changes. Besides, for a certain detection threshold, the smoothing of the measurements can shorten the duration of the detected stance phases, which will further affect the ZUPT accuracy.

B. Detection Threshold Parameter

When the detection statistic S_ω is calculated, it is compared with a detection threshold T_d to identify the stance phases. As shown in Fig. 6, the influence of the measurement fluctuations on the stance-phase detection differs when comparing S_ω with varying T_d, and the choice of T_d can also affect the duration of the detected stance phases. Normally, a higher T_d results in longer ZUPT periods and higher sensitivity to the measurement dips that occur during the swing phases; a lower T_d results in shorter ZUPT periods and higher sensitivity to the measurement rises that occur during the stance phases.

Close examination of the measurement fluctuations suggests that the choice of T_d can be guided by dividing its range into six subranges ($R_i, i = 1, 2, \cdots, 6$) as illustrated in Fig. 7. The subranges are delimited by five key thresholds ($T_{di}, i = 1, 2, \cdots, 5$) extracted from five extreme points ($S_i, i = 1, 2, \cdots, 5$). The five key thresholds are defined as

$$\begin{cases} T_{d1} = \max(\min(S_\omega^{\text{stance}})) \\ T_{d2} = \max(\max(S_\omega^{\text{stance}})) \\ T_{d3} = \min(\min(S_\omega^{\text{swing}})) \\ T_{d4} = \max(\max(S_\omega^{\text{swing}})) \\ T_{d5} = \min(\max(S_\omega^{\text{cycle}})) \end{cases} \tag{10}$$

where S_ω^{stance} and S_ω^{swing} are the detection statistics of the midstance and midswing, respectively, and S_ω^{cycle} is the detection statistic of the entire gait cycle.

The detection method has distinct properties when choosing the threshold from different subranges, which also helps to understand the roles of the five key thresholds although their exact values are not the focus.

1) $T_d \in R_1$: One or more stance phases are miss detected, and the foot is thought to be swing during these phases.
2) $T_d \in R_2$: One or more stance phases are interrupted by the measurement rise induced false swing phases.
3) $T_d \in R_3$: No measurement fluctuations exist, and, thus, no false or miss detection occurs.
4) $T_d \in R_4$: One or more measurement dips during the swing phases are detected as false stance phases.
5) $T_d \in R_5$: All the swing phases are miss detected and regarded as parts of their subsequent stance phases.
6) $T_d \in R_6$: One or more strides are miss detected, and the foot is thought to be stationary during these periods.

Terminologically, a stride refers to a gait cycle starting with the HS event, which consists of two consecutive steps [27]. In this paper, these terms are used interchangeably. Define N_d and N as the numbers of detected and actual strides, respectively. There is $N_d = N$ when $T_d \in R_3 \cup R_5$. However, when $T_d \in R_5$, the method no longer works as a stance-phase detector but just a pedometer. At first glance, R_3 appears to be the desired subrange of T_d. Unfortunately, it is hard to properly choose T_d from R_3, and R_3 does not even exist when the measurement dips to very low values during the swing phase, resulting in $T_{d3} < T_{d2}$. Moreover, although S_ω features an increasing relationship between W and R_3, as observed in Fig. 6, one should not arbitrarily increase W for a wider R_3 due to the disadvantages mentioned in Section IV-A.

C. Time Heuristic Parameter

Usually, the false gait phases are relatively short lasting. A clustering technique can be used to automatically partition the raw gait phases according to their time duration as illustrated in Fig. 8. Since the number of clusters is known, the K-means algorithm is chosen due to its simplicity and efficiency. The minimum duration of true cluster and the maximum duration of

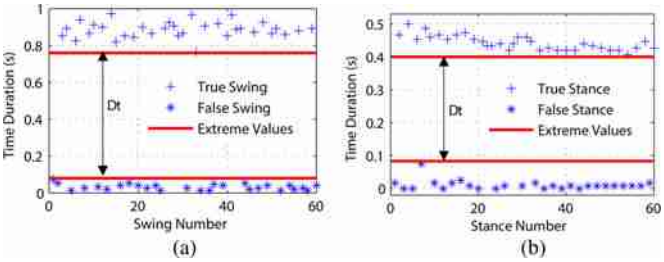

Fig. 8. Classification of the raw gait phases according to their time duration. (a) $T_d \in R_2$ with false swing phases. (b) $T_d \in R_4$ with false stance phases.

false cluster, obtained during the clustering process, are shown in Fig. 8. The time heuristic parameter Δt can be determined to be any value between these two extreme values.

However, the raw swings may not be separated by their time duration when $T_{d3} < T_{d2}$ with no R_3, because there exists a range $R = R_4 \bigcap (R_1 \bigcup R_2)$ in which the measurement rise induced false swings and the measurement dip interrupted true swings are coexistent and both short lasting. Fortunately, as the false swings normally occur when $T_d < T_{d2}$, they can be recognized by their relatively small magnitude. In this case, the magnitude of the raw swings is recommended to be examined as well. Then, the main task of the ADM method is to provide an adaptive Δt to separate the potential stance phases.

D. Detection Parameter Analysis

The objective of the stance-phase detection is to determine the suitable ZUPT periods. The three detection parameters work together to achieve this goal. The navigation accuracy depends on the integrity and validity of the detected ZUPT periods. For a given pedestrian dataset, the most suitable ZUPT periods are fixed, especially their end times. This is because the errors caused by the inaccuracy of the ZUPT start time can be corrected during this ZUPT period, whereas the errors induced by its end time inaccuracy will accumulate until the next ZUPT period begins.

In the literature review, the detection parameters have been rarely determined by quantitative criteria but tuned empirically and independently in an ad hoc manner [24], [28]. The optimal detection parameters are highly dependent on the particular application and the specific system implementation. Therefore, it is difficult to determine universal parameters for stance-phase detection. Even though some numerical values are given, further parameter tuning is necessary. This paper suggests a systematic tuning method for the time heuristic parameter Δt, which can be used as a quantitative criterion. For the window size W and the detection threshold T_d, although they are still determined by qualitative criteria and cannot be automatically chosen yet, the relationship between them is revealed and the effects of them are compared, so as to offer some suggestions on the parameter tuning, as detailed in the following.

V. Detection Method Evaluation

In this section, the detection methods are evaluated with three performance indexes, respectively.

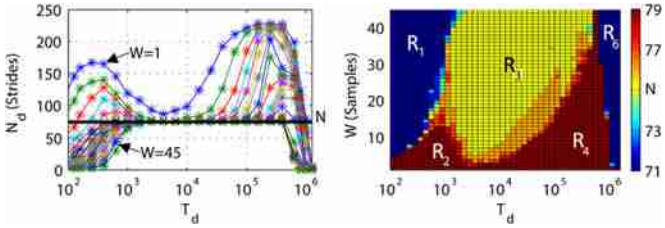

Fig. 9. Number of detected strides for the STM method.

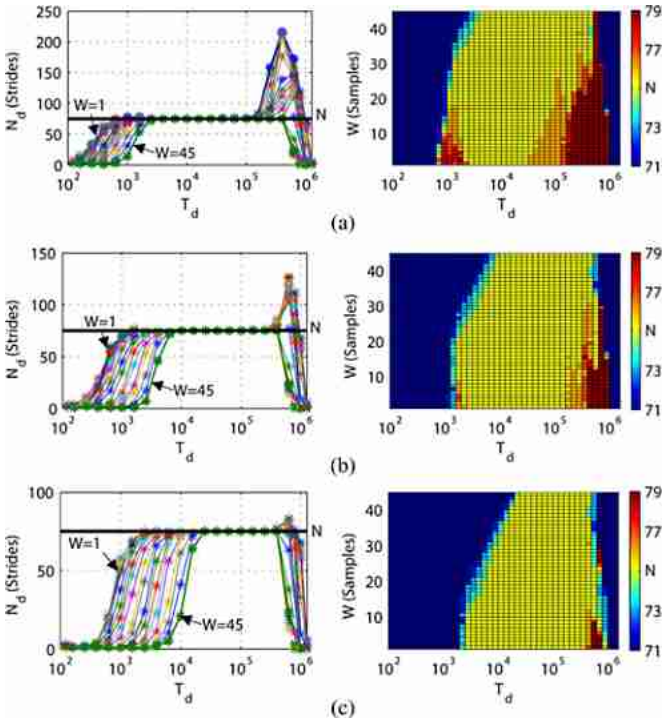

Fig. 10. Number of detected strides for the FHM method with three increasing time threshold Δt. (a) $\Delta t = 0.1$ s. (b) $\Delta t = 0.2$ s. (c) $\Delta t = 0.3$ s.

A. Number of the Detected Strides

For a 75-stride random walk, the number N_d of strides is detected by the three detection methods over a large parameter space as presented in Figs. 9–11, respectively. In each figure, the left side is the front view, and the right side is the top view. All the T_d-axes are on a logarithmic scale, so that the results for the low T_d can also be visualized.

For the STM method, the regions of all the subranges of T_d are marked in Fig. 9, except the region of R_5, which is barely visible due to the logarithmic scale. Note that, for the same reason, the region of R_3 is actually smaller than appears, and the region of R_4 is actually larger than appears. As shown in Fig. 9, R_2 and R_4 are characterized by lots of false gait phases that result in $N_d > N$. The smaller the value of W, the more the false gait phases. A further consequence is that R_3 may not even exist, which is consistent with the previous analysis.

For the FHM method, the parameter Δt is set to three increasing values. As seen in Fig. 10, a small Δt cannot filter out the relatively long false stance phases in the region of R_4,

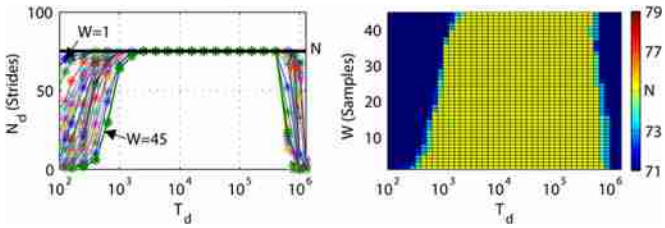

Fig. 11. Number of detected strides for the ADM method.

whereas a large Δt eliminates too many short or interrupted true stance phases in the low T_d region. Therefore, this method cannot adaptively adjust the parameter Δt to accommodate for the stance phases detected with different W and T_d, and cannot correctly handle the false swing phases without causing any miss detections of the stance phases. A fixed compromise value $\Delta t = 0.2$ s will be chosen for the FHM method, which induces some miss detections, while still eliminating large parts of the false detections.

For the ADM method, the parameter Δt is adaptively determined for each pair of W and T_d. As shown in Fig. 11, the false detections caused by the STM method are filtered out, and the miss detections caused by the FHM method are avoided. There is no longer $N_d > N$, and the flat region of $N_d = N$ over which the detection method seems to function well are extended to $T_d \in R_2 \cup R_3 \cup R_4 \cup R_5$. The detection results show that the ADM method outperforms the STM and FHM methods in detecting the stance phases in the presence of measurement fluctuations.

B. Final Return Position Estimation

For a 60-m closed-loop walk, the absolute return position error E_a is estimated for the three detection methods as presented in Fig. 12. The return position error is quantified by the difference between the initial and final positions of the estimated trajectory, and smaller values indicate less drift, which can be computed as

$$E_a = \sqrt{E_x^2 + E_y^2} \tag{11}$$

where E_x is the position error in the X-direction, and E_y is the position error in the Y-direction.

The false detection of stance-phases results in wrong ZUPT correction, while the miss detection of stance-phases leads to long period of free-inertial navigation, both of which can introduce large navigation errors, as shown in Fig. 12. In terms of the return position error, the ADM method outperforms the STM method in the small W region as the false detections are filtered out, and outperforms the FHM method in the low T_d region as the miss detections are avoided.

In the high-T_d region, the swing phases are either truncated at both ends or entirely miss detected. The ZUPT periods are extremely extended and less drift is experienced. Thus, E_a decreases toward zero when T_d increases beyond a certain level. However, such a decrease is meaningless because large distance errors occur in this region as discussed below.

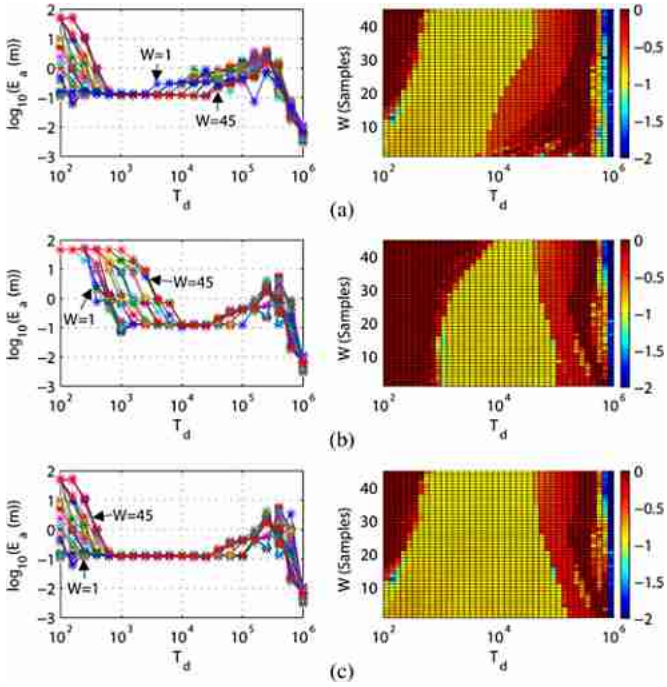

Fig. 12. Return position errors for the three detection methods. (a) STM method. (b) FHM method. (c) ADM method.

C. Total Walked Distance Estimation

Define D_d and D as the estimated and actual total walked distance, respectively. The value of D_d could be different depending on whether it is calculated per measurement or per stride. Since the estimated trajectory features kink-like or zigzag discontinuities when the ZUPT corrections are applied, especially for the wrong ZUPT correction, the D_d calculated per measurement is always longer than that calculated per stride. In this paper, D_d is calculated per stride to reduce the influence of the ZUPT-induced discontinuities.

For a 100-m straight-line walk, the walked distance D_d is estimated for the three detection methods as presented in Fig. 13. It can be observed that the false and miss detections of the stance phases may introduce large navigation errors that make $D_d > D$. The estimation results show that the ADM method outperforms the STM and FHM methods in estimating the total walked distance over a wider parameter space.

As discussed above, the detected swing phases become shorter as T_d increases, which makes the stride length progressively underestimated. Thus, D_d should exhibit a decrease along the T_d-axis. What is more, D_d even decreases to zero when T_d becomes large enough, which is not shown for clarity since all the D_d-axes are on a linear scale.

VI. Experimental Details

In this section, the setup and results of the experiments are first presented. Then, the optimal detection parameters with respect to the estimation accuracy are analyzed. Finally, some discussions on the experimental results are made.

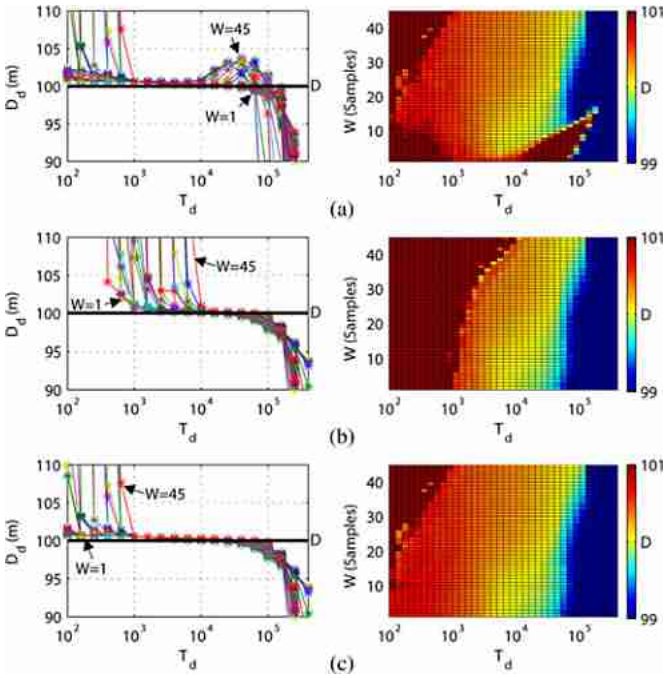

Fig. 13. Total walked distances for the three detection methods. (a) STM method. (b) FHM method. (c) ADM method.

A. Experimental Setup

Extensive experiments were conducted inside a building, and the closed-loop trajectories were chosen to cancel out the effects of initial heading alignment errors. The start position was the same for all the experiments and corresponded to the origin of the n-frame. Each experiment was repeated five times with clockwise (CW) initial direction and five times with counterclockwise (CCW) initial direction. Prior to each trial, the system was kept stationary for 20 s to estimate the sensor biases and the initial orientation of the b-frame relative to the n-frame. At the end of each trial, the dominant foot on which the senor was mounted returned to its start position.

The experiments were first conducted by one subject at varying walking speeds along a 60-m rectangular trajectory (Test #1). The subject was instructed to walk in time with a metronome beat at five cadences, representing very slow, slow, normal, fast, and very fast gaits. During this stage, 50 datasets were collected to study the effect of gait speed on the choice of detection parameters. The experiments were then extended to include six subjects (three males and three females) for a richer data collection, and the subjects were asked to walk at self-selected speeds along a 120-m figure-of-eight trajectory (Test #2). During this stage, another 60 datasets were collected to increase the variability of the gait data and prove the robustness of the proposed detection method.

B. Experimental Results

1) Overall Experimental Performance: The performances of the three detection methods are evaluated with all the datasets. The performance indexes are calculated as a function of the window size W and the detection threshold T_d. The parameter space is taken to be $W \in [1, 45]$ and $T_d \in \left[10^2, 10^6\right]$, where W forms an arithmetic sequence, while T_d forms a geometric sequence. The experimental results are compared from two aspects: the number of the feasible parameter pairs and the area of the feasible parameter space, which are denoted by Count$(\cdot)$ and Area$(\cdot)$, respectively. Table II summarizes the percentage of the detection results with $N_d = N$.

TABLE II
RELIABILITY OF THE STANCE-PHASE DETECTION (%)

Test		$Count(N_d = N)$			$Area(N_d = N)$		
		STM	FHM	ADM	STM	FHM	ADM
#1	90 (steps/min)	42.64	60.34	76.65	19.85	58.15	66.19
	100 (steps/min)	44.42	54.69	74.01	24.48	62.80	68.94
	110 (steps/min)	49.74	49.91	73.90	28.57	66.54	67.92
	120 (steps/min)	48.48	41.66	68.11	29.31	65.68	68.54
	130 (steps/min)	48.13	38.68	69.38	35.44	80.31	83.99
#2	Subject #1	47.64	47.29	77.54	17.68	47.33	52.11
	Subject #2	15.62	33.82	60.45	9.11	29.47	40.31
	Subject #3	27.40	30.97	54.62	14.74	35.27	38.84
	Subject #4	31.76	42.40	69.35	9.48	34.87	46.59
	Subject #5	40.76	49.07	80.97	15.56	46.29	53.86
	Subject #6	46.16	53.22	76.13	25.64	64.94	72.17
	Average	40.25	45.64	71.01	20.90	53.79	59.95

TABLE III
RELIABILITY OF THE RETURN POSITION ESTIMATION (%)

Test		$Count(\text{RMSE} < 1\%)$			$Area(\text{RMSE} < 1\%)$		
		STM	FHM	ADM	STM	FHM	ADM
#1	90 (steps/min)	67.06	60.39	74.11	18.86	25.99	26.07
	100 (steps/min)	68.06	55.67	74.67	18.29	28.10	28.29
	110 (steps/min)	69.56	49.94	75.99	21.07	28.63	29.47
	120 (steps/min)	67.83	40.89	72.22	22.79	28.86	29.55
	130 (steps/min)	66.78	36.50	71.72	27.90	35.72	37.06
#2	Subject #1	73.94	57.39	81.94	19.88	31.60	32.02
	Subject #2	54.02	42.78	63.50	5.66	8.70	9.04
	Subject #3	53.44	32.94	59.28	16.30	21.31	22.96
	Subject #4	60.28	44.13	72.22	6.71	11.84	16.01
	Subject #5	58.33	42.22	83.11	15.59	19.15	34.96
	Subject #6	73.00	57.23	79.33	28.58	39.83	40.07
	Average	64.76	47.28	73.46	18.33	25.43	27.77

To eliminate the dependence of the estimation results on the trajectory length, relative performance indexes are derived as

$$E_{\text{rp}} = \sqrt{E_x^2 + E_y^2}/D$$
$$E_{\text{rd}} = |D_d - D|/D \tag{12}$$

where E_{rp} is the relative return position error, and E_{rd} is the relative walked distance error.

The root-mean-square values of E_{rp} and E_{rd} are calculated, which can be interpreted as the relative root-mean-square errors (RMSE) of the position and distance estimation results, respectively. Table III summarizes the percentage of the position estimates with RMSE $< 1\%$, while Table IV summarizes the percentage of the distance estimates with RMSE $< 1\%$.

TABLE IV
RELIABILITY OF THE WALKED DISTANCE ESTIMATION (%)

Test		$Count$(RMSE< 1%)			$Area$(RMSE< 1%)		
		STM	FHM	ADM	STM	FHM	ADM
#1	90 (steps/min)	46.94	42.78	56.61	11.38	10.56	10.73
	100 (steps/min)	49.56	37.89	55.56	11.09	10.42	10.80
	110 (steps/min)	52.89	34.44	56.89	12.67	11.42	12.16
	120 (steps/min)	52.50	29.33	55.56	15.46	13.76	14.91
	130 (steps/min)	47.56	23.72	49.61	19.91	16.87	20.23
#2	Subject #1	54.94	37.94	57.94	13.05	12.29	13.20
	Subject #2	39.11	31.33	50.00	6.62	5.44	5.73
	Subject #3	36.89	18.44	41.61	8.25	6.28	8.41
	Subject #4	16.33	18.94	19.44	9.92	10.95	11.13
	Subject #5	45.28	29.00	57.33	17.23	18.67	22.44
	Subject #6	52.89	39.56	59.17	13.50	12.06	12.51
	Average	44.99	31.22	50.88	12.64	11.70	12.93

TABLE V
EXPERIMENTAL PERFORMANCE OF THE PROPOSED METHOD (%)

Test		E_{rp}		E_{rd}	
		Mean	Standard Deviation	Mean	Standard Deviation
#1	90 (steps/min)	0.17	0.10	0.20	0.12
	100 (steps/min)	0.16	0.09	0.36	0.20
	110 (steps/min)	0.12	0.05	0.41	0.19
	120 (steps/min)	0.15	0.07	0.29	0.19
	130 (steps/min)	0.14	0.06	0.15	0.12
#2	Subject #1	0.20	0.10	0.25	0.16
	Subject #2	0.33	0.19	0.10	0.06
	Subject #3	0.47	0.21	0.21	0.14
	Subject #4	0.49	0.20	0.43	0.19
	Subject #5	0.42	0.29	0.17	0.12
	Subject #6	0.21	0.11	0.17	0.11
	Average	0.26	0.13	0.25	0.15

Tables II–IV summarize the overall experimental results for the three detection methods. Although the values given in these tables will change as the parameter space changes, they still indicate the improvement of the ADM method over the STM and FHM methods, in not only the stance-phase detection but also the position and distance estimations.

2) Best Experimental Performance: Table V gives the best experimental results for the ADM method, which are the minimum estimation errors of the return position and walked distance. With the detection parameters that yield the best experimental results, the walking trajectories are estimated and mapped onto the floor plan of the building as shown in Fig. 14. It can be observed that the estimated trajectories match well with the layout of the floor plan.

The close-ups of the estimated final positions are shown in Fig. 15. For the rectangular trajectory, due to the relatively short walking time, the sensor measurement errors did not contribute much to the system, and, therefore, the errors in the X- and Y-directions are similar. However, for the figure-of-eight trajectory, the errors in the Y-direction are larger than that in the X-direction. This is probably because, for the sensor that

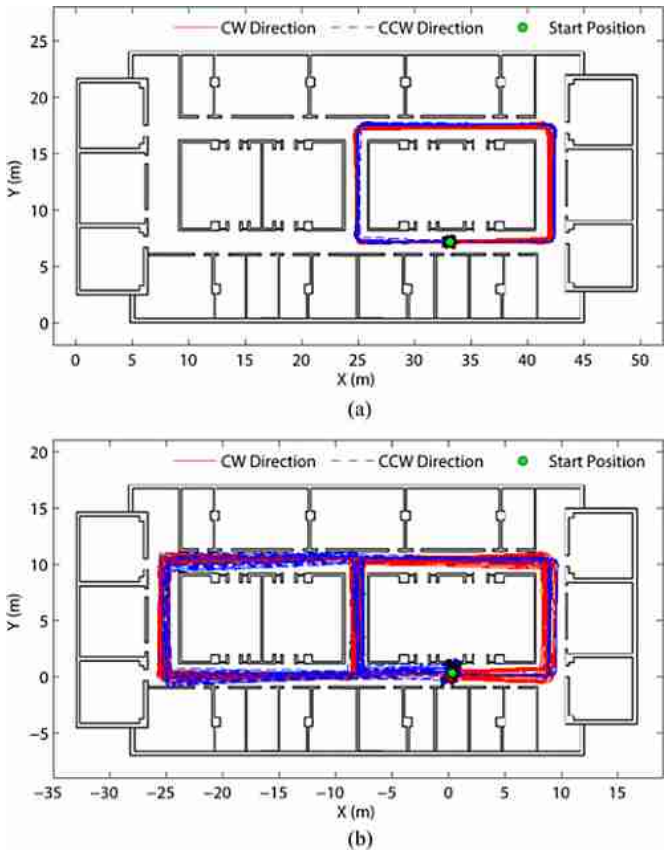

Fig. 14. Estimated walking trajectories. (a) Test #1: Small rectangular trajectory. (b) Test #2: Figure-of-eight trajectory.

we have, the gyroscope measurement errors are the dominant error sources affecting the positioning accuracy. The position errors can be decomposed into lateral and longitudinal parts with respect to the walking direction. As the trajectory in the X-direction is longer than that in the Y-direction, and the larger error components happen to be perpendicular to the X-direction, it is suggested that the lateral errors are the major part of the position errors, which in turn are mainly caused by the gyroscope measurement errors. The longer the trajectory in one direction, the more obvious this phenomenon.

Furthermore, as observed in Fig. 15, the walking direction has little effect on the position estimation. The final positions neither tend to gather at one side of the start position nor scatter symmetrically about the start position for the opposite walking directions. This suggests that the sensor biases could be effectively estimated prior to each trial, and the navigation errors are likely due to the random noises of the sensor and the modeling errors in the system.

C. Optimal Detection Parameters

The average values of the optimal detection parameters W and T_d for different walking speeds and different subjects are presented in Fig. 16. It can be observed that the optimal T_d increases with increasing W, which verifies the discussion in Section IV that the changes of W and T_d have opposite effects

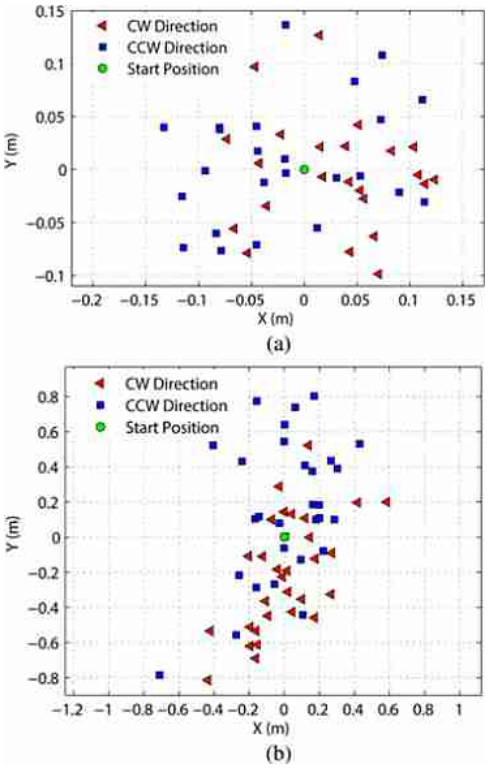

Fig. 15. Final positions of the estimated walking trajectories. (a) Test #1: Small rectangular trajectory. (b) Test #2: Figure-of-eight trajectory.

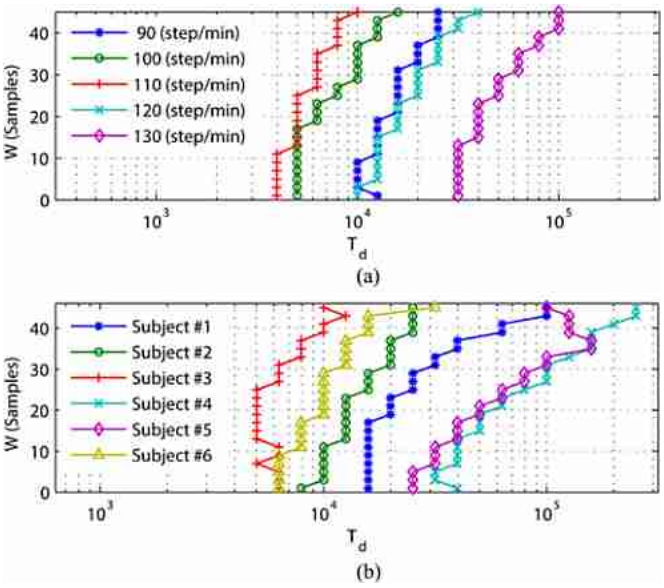

Fig. 16. Relationship between optimal detection parameters: W versus T_d. (a) Test #1: One subject at five fixed walking speeds. (b) Test #2: Six subjects at self-selected walking speeds.

on the time duration of the detected ZUPT periods, and the most suitable ZUPT periods (at least their end times) are relatively fixed for a given dataset. In this sense, the system performance should be somewhat independent of the window size W as shown in Fig. 17 for the position error E_a. This is different from

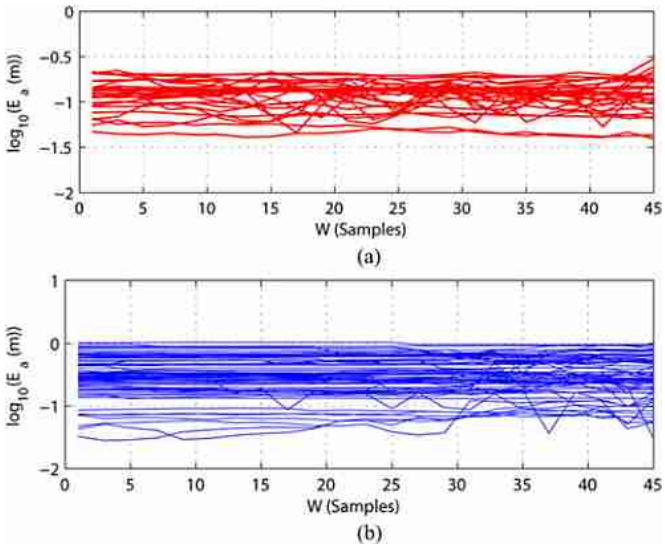

Fig. 17. Minimum absolute return position error E_a versus window size W. (a) Test #1: One subject at five fixed walking speeds. (b) Test #2: Six subjects at self-selected walking speeds.

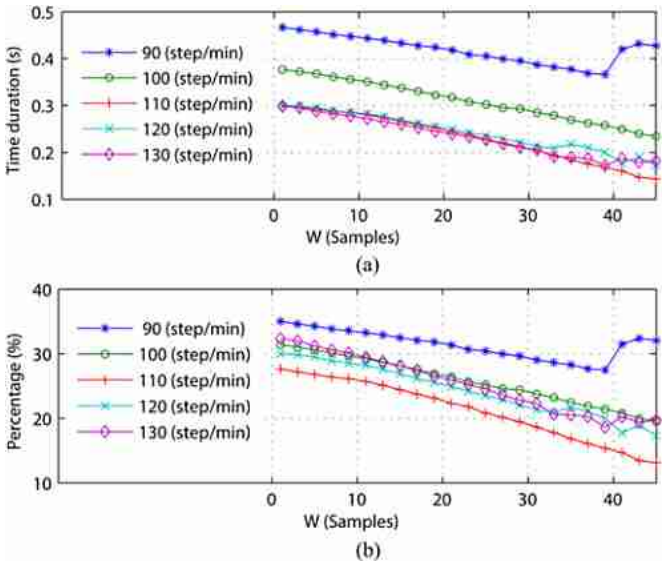

Fig. 18. Optimal ZUPT period versus gait speed and window size W. (a) Time duration of the optimal ZUPT periods. (b) Percentages of the optimal ZUPT periods in the gait cycles.

the findings in [13], where the measurement fluctuations were not considered.

In general, if the foot is subjected to slow movement, the ZUPT periods would be relatively long; if the foot movement is fast, the ZUPT periods would be relatively short as shown in Fig. 18(a). However, the percentage of the ZUPT periods in each gait cycle shows a limited dependence on the gait speed as shown in Fig. 18(b). Note that the time duration of the optimal ZUPT periods decreases as the window size increases. A close examination of these ZUPT periods reveals that this is mainly due to the shifts of their start times, whereas their end times change little with the window size, which is consistent with the previous discussion.

Among the three detection parameters, Δt can be automatically determined by the detection method proposed in this paper, W has little effect on the system performance, whereas T_d is a necessary parameter that still needs to be chosen carefully. Fortunately, when the false gait phases are effectively filtered out, the feasible parameter space can be greatly extended, which allows the system to work over a wider parameter space and makes the choice of W and T_d more flexible. We recommend setting W, then adjusting T_d. For example, setting $W = 1$ to derive the detection statistic from the measurement magnitude with no time delay and no signal distortion, then adjusting T_d to make the ZUPT periods constitute roughly 30% of the gait cycles.

D. Discussion

It is found that no single performance index can fully evaluate the detection methods. The return position error cannot explain the distance scaling errors, the distance error cannot explain the heading drift errors, and both of them cannot account for the discontinuities of the estimated trajectory induced by false or miss detections of the stance phases. These discontinuities could lead to the deviation of other positions from the walking trajectory except the final position. Thus, E_a features a decrease in the high-T_d region, whereas D_d exhibits a local increase as T_d decreases as shown in Figs. 12 and 13(a), respectively. In terms of the walked distance estimation, this local increase of D_d causes the improvement of the ADM method over the STM method to not always hold true as seen in Table IV. Therefore, the correct stance-phase detection is crucial for the ZUPT-aided IPNS, which makes the estimated trajectories closer to the ground truth and smoother without abrupt discontinuities. The proposed detection method can deal with the measurement fluctuations more robustly, and allows finding the optimal detection parameters over a wider parameter space.

With no pressure sensor for the stance-phase detection and no magnetic sensor for the heading drift prevention, the pure ZUPT-aided IPNS can achieve an average position error of 0.26% and an average distance error of 0.25% in an indoor environment. It is difficult to directly compare the results from different experiments, since the system performance is dependent on several factors, such as the system setup, the ground surface, and the trajectory characteristic. Even though, our experimental results are comparable to or better than some of the best results reported in the literature.

1) With the same IMU, the position error of 0.35% for normal walk and 0.56% for fast walk were reported in [29]; the distance error of 0.3% for slow walk and 0.8% for fast walk, the position error of 0.9% in CW direction and 0.6% in CCW direction were reported in [7]; the distance error of 5.5% in indoor laboratory and 1.3% in outdoor environment were reported in [30].
2) With other IMUs, the distance error of 1.1% and the position error of 1.2% were reported in [20] and [31]; the position error of 0.82% and the distance error of 0.27% were reported in [12]; the position error of 0.14% for normal gait and 0.3% for fast gait were reported in [13]; the position error of 0.4% was reported in [21] and [24].

VII. Conclusion and Future Work

This paper has described a stance-phase detection method for the ZUPT-aided PNS using a sole foot-mounted IMU. A clustering algorithm is used to partition the potential gait phases into true and false groups, thereby yielding an adaptive time heuristic parameter to eliminate the false gait phases. We demonstrate how the system performance changes as the detection parameters change, and what system improvement can be achieved by appropriately tuning of the detection parameters.

The proposed detection method has been compared with the two existing methods, by examining not only the number of the detected strides but also the estimation errors of the return position and walked distance. The three detection methods have been evaluated with multisubject experimental data collected at controlled and self-selected walking speeds. The evaluation results demonstrate that the proposed method makes the system performance more robust to the measurement fluctuations and the detection parameters.

In future work, we will extend our method for other modes of pedestrian locomotion, such as sidestepping, running, and climbing. Moreover, reasonable indexes will be explored to evaluate the system performance as fully as possible.

References

[1] L. Marín, M. Vallés, Á. Soriano, Á. Valera, and P. Albertos, "Event-based localization in Ackermann steering limited resource mobile robots," *IEEE/ASME Trans. Mechatronics*, vol. 19, no. 4, pp. 1171–1182, Aug. 2014.

[2] K. Wang, Y. H. Liu, and L. Y. Li, "A simple and parallel algorithm for real-time robot localization by fusing monocular vision and odometry/AHRS sensors," *IEEE/ASME Trans. Mechatronics*, vol. 19, no. 4, pp. 1447–1457, Aug. 2014.

[3] H. Fourati, N. Manamanni, L. Afilal, and Y. Handrich, "Complementary observer for body segments motion capturing by inertial and magnetic sensors," *IEEE/ASME Trans. Mechatronics*, vol. 19, no. 1, pp. 149–157, Feb. 2014.

[4] H. Y. Zhao, Z. L. Wang, H. Shang, W. J. Hu, and G. Qin, "A time-controllable Allan variance method for MEMS IMU," *Ind. Robot, Int. J.*, vol. 40, no. 2, pp. 111–120, 2013.

[5] H. Hur and H. S. Ahn, "Unknown input H_∞ observer-based localization of a mobile robot with sensor failure," *IEEE/ASME Trans. Mechatronics*, vol. 19, no. 6, pp. 1830–1838, Dec. 2014.

[6] G. Panahandeh and M. Jansson, "Vision-aided inertial navigation based on ground plane feature detection," *IEEE/ASME Trans. Mechatronics*, vol. 19, no. 4, pp. 1206–1215, Aug. 2014.

[7] L. Ojeda and J. Borenstein, "Non-GPS navigation for security personnel and first responders," *J. Navig.*, vol. 60, no. 3, pp. 391–407, Sep. 2007.

[8] Ö. Bebek, M. A. Suster, S. Rajgopal, M. J. Fu, X. M. Huang, M. C. Çavuşoğlu, D. J. Young, M. Mehregany, A. J. van den Bogert, and C. H. Mastrangelo, "Personal navigation via high-resolution gait-corrected inertial measurement units," *IEEE Trans. Instrum. Meas.*, vol. 59, no. 11, pp. 3018–3027, Nov. 2010.

[9] A. R. Jiménez, F. Seco, J. C. Prieto, and J. Guevara, "Indoor pedestrian navigation using an INS/EKF framework for yaw drift reduction and a foot-mounted IMU," in *Proc. 7th Workshop Positioning Navig. Commun.*, Dresden, Germany, Mar. 2010, pp. 135–143.

[10] C. Fischer, P. T. Sukumar, and M. Hazas, "Tutorial: Implementing a pedestrian tracker using inertial sensors," *IEEE Pervasive Comput.*, vol. 12, no. 2, pp. 17–27, Apr./Jun. 2013.

[11] R. Feliz, E. Zalama, and J. G. García-Bermejo, "Pedestrian tracking using inertial sensors," *J. Phys. Agents*, vol. 3, no. 1, pp. 35–42, Jan. 2009.

[12] X. P. Yun, J. Calusdian, E. R. Bachmann, and R. B. McGhee, "Estimation of human foot motion during normal walking using inertial and magnetic sensor measurements," *IEEE Trans. Instrum. Meas.*, vol. 61, no. 7, pp. 2059–2072, Jul. 2012.

[13] I. Skog, J. O. Nilsson, and P. Handel, "Evaluation of zero-velocity detectors for foot-mounted inertial navigation systems," in *Proc. Int. Conf. Indoor Positioning Indoor Navig.*, Zurich, Switzerland, Sep. 2010, pp. 1–6.

[14] C. Zhou, J. Downey, J. Choi, D. Stancil, J. Paramesh, and T. Mukherjee, "A shoe-embedded RF sensor for motion detection," *IEEE Microw. Wireless Compon. Lett.*, vol. 21, no. 3, pp. 169–171, Mar. 2011.

[15] J. O. Nilsson, I. Skog, and P. Händel, "A note on the limitations of ZUPTs and the implications on sensor error modeling," in *Proc. Int. Conf. Indoor Positioning Indoor Navig.*, Sydney Australia, Nov. 2012, pp. 1–4.

[16] P. Strömbäck, J. Rantakokko, S. L. Wirkander, M. Alexandersson, I. Fors, I. Skog, and P. Händel, "Foot-mounted inertial navigation and cooperative sensor fusion for indoor positioning," in *Proc. Int. Tech. Meet. Inst. Navig.*, San Diego, CA, USA, Jan. 2010, pp. 89–98.

[17] K. Abdulrahim, C. Hide, T. Moore, and C. Hill, "Integrating low cost IMU with building heading in indoor pedestrian navigation," *J. Global Positioning Syst.*, vol. 10, no. 1, pp. 30–38, 2011.

[18] X. L. Meng, S. Y. Sun, L. Y. Ji, J. K. Wu, and W. C. Wong, "Estimation of center of mass displacement based on gait analysis," in *Proc. Int. Conf. Body Sens. Netw.*, Dallas, TX, USA, May 2011, pp. 150–155.

[19] K. Abdulrahim, C. Hide, T. Moore, and C. Hill, "Aiding MEMS IMU with building heading for indoor pedestrian navigation," in *Proc. Ubiquitous Positioning Indoor Navig. Location Based Service Conf.*, Kirkkonummi, Finland, Oct. 2010, pp. 1–6.

[20] S. Godha and G. Lachapelle, "Foot mounted inertial system for pedestrian navigation," *Meas. Sci. Technol.*, vol. 19, no. 7, pp. 1–9, Jul. 2008.

[21] H. Fourati, "Heterogeneous data fusion algorithm for pedestrian navigation via foot-mounted inertial measurement unit and complementary filter," *IEEE Trans. Instrum. Meas.*, vol. 64, no. 1, pp. 149–157, Jan. 2015.

[22] I. Skog, P. Handel, J. O. Nilsson, and J. Rantakokko, "Zero-velocity detection—An algorithm evaluation," *IEEE Trans. Biomed. Eng.*, vol. 57, no. 11, pp. 2657–2666, Nov. 2010.

[23] Memsense. (2013). Nano IMU product specification and user's guide. [Online]. Available: http://www.memsense.com

[24] X. L. Meng, Z. Q. Zhang, J. K. Wu, W. C. Wong, and H. Y. Yu, "Self-contained pedestrian tracking during normal walking using an inertial/magnetic sensor module," *IEEE Trans. Biomed. Eng.*, vol. 61, no. 3, pp. 892–899, Mar. 2014.

[25] A. Mannini and A. M. Sabatini, "Gait phase detection and discrimination between walking-jogging activities using hidden Markov models applied to foot motion data from a gyroscope," *Gait Posture*, vol. 36, no. 4, pp. 657–661, Sep. 2012.

[26] D. Kotiadis, H. J. Hermens, and P. H. Veltink, "Inertial gait phase detection for control of a drop foot stimulator: Inertial sensing for gait phase detection," *Med. Eng. Phys.*, vol. 32, no. 4, pp. 287–297, May 2010.

[27] E. Ayyappa, "Normal human locomotion, part 1: Basic concepts and terminology," *J. Prosthetics Orthotics*, vol. 9, no. 1, pp. 10–17, 1997.

[28] J. O. Nilsson, I. Skog, and P. Händel, "Performance characterisation of foot-mounted ZUPT-aided INSs and other related systems," in *Proc. Int. Conf. Indoor Positioning Indoor Navig.*, Zurich, Switzerland, Sep. 2010, pp. 1–7.

[29] L. Ojeda and J. Borenstein, "Non-GPS navigation with the personal dead-reckoning system," in *Proc. SPIE Def. Security Conf., Unmanned Syst. Technol. IX*, Orlando, FL, USA, Apr. 2007, vol. 6561, pp. 1–11.

[30] X. P. Yun, E. R. Bachmann, H. Moore IV, and J. Calusdian, "Self-contained position tracking of human movement using small inertial/magnetic sensor modules," in *Proc. IEEE Int. Conf. Robot. Autom.*, Roma, Italy, Apr. 2007, pp. 2526–2533.

[31] S. Godha, G. Lachapelle, M. E. Cannon, and Navstar,, "Integrated GPS/INS system for pedestrian navigation in a signal degraded environment," in *Proc. 19th Int. Tech. Meet. Satellite Div. Inst. Navigat.*, Fort Worth, TX, USA, Sep. 2006, pp. 2151–2164.

Zhelong Wang (M'04) received the B.S. and M.S. degrees in automatic control from the Dalian University of Technology, Dalian, China, in 1996 and 1999, respectively, and the Ph.D. degree in robotics from the University of Durham, Durham, U.K., in 2003.

In 2004, he joined the School of Electronic and Information Engineering, Dalian University of Technology, where he is currently a Professor. His research interests include robotics, intelligent control, mechatronics, body sensor networks, and machine learning.

Hongyu Zhao received the B.S. degree in automation from the Dalian University of Technology, Dalian, China, in 2007, where she has been working toward the Ph.D. degree in control theory and control engineering with the School of Control Science and Engineering since 2009.

Her current research interests include pedestrian navigation, indoor localization, inertial navigation and positioning, and gait analysis.

Sen Qiu received the B.S. degree in automation from the Dalian University of Technology, Dalian, China, in 2009, where he has been working toward the Ph.D. degree in control theory and control engineering with the School of Control Science and Engineering since 2011.

He was a Visiting Researcher at the Department of Computer Science and Electronic Engineering, University of Essex, Colchester, U.K., from 2013 to 2014. His current research interests include gait analysis, body sensor network, and pattern recognition.

Qin Gao received the B.S. degree in automation from the North China University of Water Conservancy and Hydropower, Zhengzhou, China, in 2007, where she has been working toward the Ph.D. degree in control theory and control engineering with the School of Control Science and Engineering since 2009.

Her current research interests include bioinspired robotics, gait analysis, control and model of snake-like robot, and locomotion.